Aerocapture Design Study for a Titan Polar Orbiter

Conor A. Nixon
Planetary Systems Laboratory
NASA Goddard Space Flight Center
Greenbelt, MD 20771
301-286-6757
conor.a.nixon@nasa.gov

Frank Kirchman
Mission Systems Engineering Branch
NASA Goddard Space Flight Center
Greenbelt, MD 20771
301-286-1218
frank.j.kirchman@nasa.gov

Jaime Esper
Advanced Concepts Branch
NASA Goddard Space Flight Center
Greenbelt, MD 20771
301-286-1124
jaime.esper-1@nasa.gov

David Folta, Alinda Mashiku
Navigation and Mission Design Branch
NASA Goddard Space Flight Center
Greenbelt, MD 20771
301-286-6082, 301-286-2856
david.c.folta, alinda.k.mashiku

Abstract—In 2014 a team at NASA Goddard Space Flight Center (GSFC) studied the feasibility of using active aerocapture to reduce the chemical ΔV requirements for inserting a small scientific satellite into Titan polar orbit. The scientific goals of the mission would be multi-spectral imaging and active radar mapping of Titan's surface and subsurface. The study objectives were to: (i) identify and select from launch window opportunities and refine the trajectory to Titan; (ii) study the aerocapture flight path and refine the entry corridor; (iii) design a carrier spacecraft and systems architecture; (iv) develop a scientific and engineering plan for the orbital portion of the mission. Study results include: (i) a launch in October 2021 on an Atlas V vehicle, using gravity assists from Earth and Venus to arrive at Titan in January 2031; (ii) initial aerocapture via an 8-km wide entry corridor to reach an initial 350×6000 km orbit, followed by aerobraking to reach a 350×1500 km orbit, and a periapse raise maneuver to reach a final 1500 km circular orbit; (iii) a three-part spacecraft system consisting of a cruise stage, radiator module, and orbiter inside a heat shield; (iv) a 22-month mission including station keeping to prevent orbital decay due to Saturn perturbations, with 240 Gb of compressed data returned. High-level issues identified include: (i) downlink capability - realistic downlink rates preclude the desired multi-spectral, global coverage of Titan's surface; (ii) power - demise of the NASA ASRG (Advanced Stirling Radioisotope Generator) program, and limited availability at present of MMRTGs (Multi-Mission Radioisotope Generators) needed for competed outer planet missions; (iii) thermal - external radiators must be carried to remove 4 kW of waste heat from MMRTGs inside the aeroshell, requiring heat pipes that pass through the aeroshell lid, compromising shielding ability; (iv) optical navigation to reach the entry corridor; (v) the NASA requirement of continuous critical event coverage for the orbiter, especially during the peak heating of the aerocapture when the radio link will be broken. In conclusion, although Titan aerocapture allows for considerable savings in propellant mass, this comes at a cost of increased mission complexity. Further architecture study and refinement is required to reduce high-level mission risks and to elucidate the optimum architecture.

TABLE OF CONTENTS

1. INTRODUCTION

Titan, largest satellite of Saturn, is the only moon in the solar system to have a significant atmosphere, which is composed mainly of nitrogen (N_2, 95–98% depending on altitude) like that of the Earth [1]. Due to the combination of low surface gravity (1.352 m/s^2) and cold temperatures ($\sim$70-170 K), Titan has a dense but extended atmosphere, with an exobase at $\sim$1500 km [2], [3]. These conditions make Titan a near-ideal target for aerocapture - the process of capturing a spacecraft from hyperbolic flyby trajectory into elliptical orbit - by virtue of the dense, inert atmosphere and relatively large atmospheric scale height. The large scale height $H = RT/mg$ (where R=ideal gas constant, T=temperature, m=mean molecular mass of atmosphere, g=acceleration due to gravity), which is $\sim$50–60 km in the middle and upper atmosphere, around five times that of Earth or Mars, implies a useful forgivingness to trajectory uncertainties.

Over a decade ago, a joint series of studies between several NASA Centers (Ames, Glenn and JPL in particular) and partner organizations into aerocapture at Titan resulted in a set of twelve published conference proceedings at the 39th AIAA/ASME/SAE/ASEE Joint Propulsion Conference in Huntsville, AL, July 22nd 2003. Much of this work was later incorporated into a joint technical report in 2006 led by Mary Lockwood of NASA Langley [4], and several JPL authors published a separate journal article on the cost-benefit analysis of aerocapture at multiple targets (including Titan) [5]. The Lockwood report in turn became a significant input to a Titan 'flagship' (i.e. large-size) mission study commissioned by NASA and led by the Johns Hopkins University Applied Physics Laboratory [6], which emphasized aerocapture as a preferable option to chemical propulsion for enhancing delivered mass into Titan orbit.

The mission study reported here was motivated by the 2011 Decadal Survey for Planetary Sciences [7] (hereafter VV11), which appeared since the earlier mission studies were completed. In VV11, the planetary science community chose to prioritize missions to Mars, Europa and Uranus for future large flagship missions ($2bn+) in the next decade and beyond, while the target list for medium-class, 'New Frontiers'-

class ($1bn) also did not include Titan as a preferred destination. Therefore, any NASA missions to Titan through the early 2020s must conform to small, Discovery-class ($0.5bn) mission requirements. Since mission costs typically increase with increasing spacecraft dry mass, a Discovery-class mission to Titan must necessarily be small and lightweight.

The purpose of the present study was to consider whether aerocapture would serve to be mission-enabling for a Discovery-class mission to Titan, by reducing launch total (wet) mass compared to a similar mission that used chemical propulsion for orbit insertion at Titan. An aerocapture architecture can be expected to reduce wet mass dramatically through using no fuel for the major ΔV of the mission (capture into Titan orbit, several km/s), while also reducing the dry mass through reductions in tank and engine size, plus proportional decreases in structural mass. However, additional mass will be added by the need for a protective aeroshell and other mechanisms required for the aerocapture.

In this paper we summarize the Titan Orbiter Polar Surveyor (TOPS) mission as designed in 2014 by the NASA Goddard Mission Design Laboratory (MDL), part of the Integrated Design Center (IDC) [8]. We will focus on giving a high-level overview of the mission including launch, flight dynamics, spacecraft systems engineering, mission operations - and the key aspect of the aerocapture in some detail. We will also mention some of the subsystems - especially power, thermal, and communications, which have aspects unique to this mission. We do not describe remaining subsystems and engineering disciplines (including avionics, flight software, mechanical, radiation, electrical other than power) which do not present novel challenges, although these were included in the mission study. Propulsion is discussed only at the mission level (ΔV required etc) rather than the engineering level. In the conclusions we re-evaluate the trade between the various mission types by propulsion, and highlight some key challenges identified by the study.

2. Science Goals and Payload

The Cassini-Huygens mission, orbiting Saturn since 2004, has provided the first detailed scientific picture of Titan during more than 100 close encounters with the moon, and the remarkable descent of Huygens through the atmosphere to the surface in January 2005. By the time the mission ends in 2017, the orbiter will have made 126 targeted encounters with Titan at ranges as low as 950 km, and used its 12 instruments to make measurements as diverse as optical imaging of the surface and atmosphere, in situ measurements of particles and fields, Synthetic Aperture Radar (SAR) mapping of the surface, and radio occultations of the atmosphere. Our knowledge of Titan has been vastly increased, and yet many questions raised as long ago as the Voyager flyby in 1980 still remain unanswered.

Titan's major mystery remains the origin and persistence of the atmosphere, in spite of continual loss due to an active photochemistry that depletes the second most abundant gas, methane. At current loss rates, the 2–5% methane will vanish entirely in ∼30–100 Myr [9], [10], leading to major changes in the existing greenhouse effect and probable cooling and collapse of the remaining nitrogen atmosphere onto the surface [11]. Only by continual methane replenishment can the atmosphere remain in a steady state over geologic time periods, leading to speculations that interior activity - episodic outgassing or cryovolcanism on large or small scales

- must be occurring [12], [13], [14], [15]. A secondary and closely related mystery to the methane resupply conundrum is the fate of the organics produced by photochemistry - the existing organic surface deposits in liquid and solid form [16] cannot account for the predicted quantities should have accumulated over the age of the solar system.

Although Cassini has revealed many new and fascinating surface features - including northern hydrocarbon seas [17] and equatorial dune fields of probable organic composition [18] - it has not managed to firmly resolve the important question regarding endogenic activity, evidence for which has been hotly debated [19]. For this reason, a Titan orbiter mission has the potential to make significant new measurements to advance our understanding of Titan's past and present activity, and to make major strides towards resolution of the questions surrounding the origin and fate of the atmosphere. In particular, a polar orbiter has the ability to make multispectral maps of the entire surface at uniform resolution, greatly improving on the patchwork coverage from Cassini (Fig. 1), and providing a key resource for understanding Titan's history.

The science traceability matrix (STM) for the conceived mission - Titan Orbiter and Polar Surveyor (TOPS) - is shown in Table 1, including details of the instrument payload.

The nominal payload for the TOPS orbiter is comprised of five instruments:

1. **Radar SAR:** an X-band radar (4 cm) working in either altimetry mode or synthetic aperture (SAR) mode.
2. **Camera/Spectrometer:** a combined visible camera system with filters, and near-IR spectral imager.
3. **Dipole radar:** a long-wavelength (1–5 MHz) radar capable of either altimetry or deep sounding modes.
4. **Magnetometer:** mounted on a 4 m boom.
5. **Radio science:** radio science including atmospheric occultation measurements using the spacecraft HGA.

3. Mission Architecture

The overall mission architecture is determined by an iterative process. It is essential to the aero-capture analysis to define a range of entry speeds and flight path angles that result in acceptable aero-capture delta-Vs and aerodynamic heat loads (and to a lesser extent decelerations). This in turn must be considered in the light of acceptable Earth departure energies and flight times to the destination. Before final selection of the technologies to execute the mission, a trade analysis on the interplanetary trajectory and propulsion system options was carried out that considered an all-chemical and a combination of solar electric (to less than 2 AU) and chemical propulsion systems. Key steps in the iteration are outlined here.

1. A number of potential flight trajectories are identified, based on desired launch date and flight time. Each trajectory may have multiple gravity assists, in this case from Venus and Earth flybys, since Jupiter is not in the right position for gravity assist to Saturn in the 2020s.
2. Resulting ΔV's from trajectory options are used to define the propulsion system needs. The higher the ΔV, the more advantageous it is to use high specific impulse (I_{sp}) systems. However, this comes at the expense of higher power system masses, and for an an outer planet mission, complexity in the need to use a staged propulsion system approach (i.e., solar electric propulsion becomes impractical at greater than, about
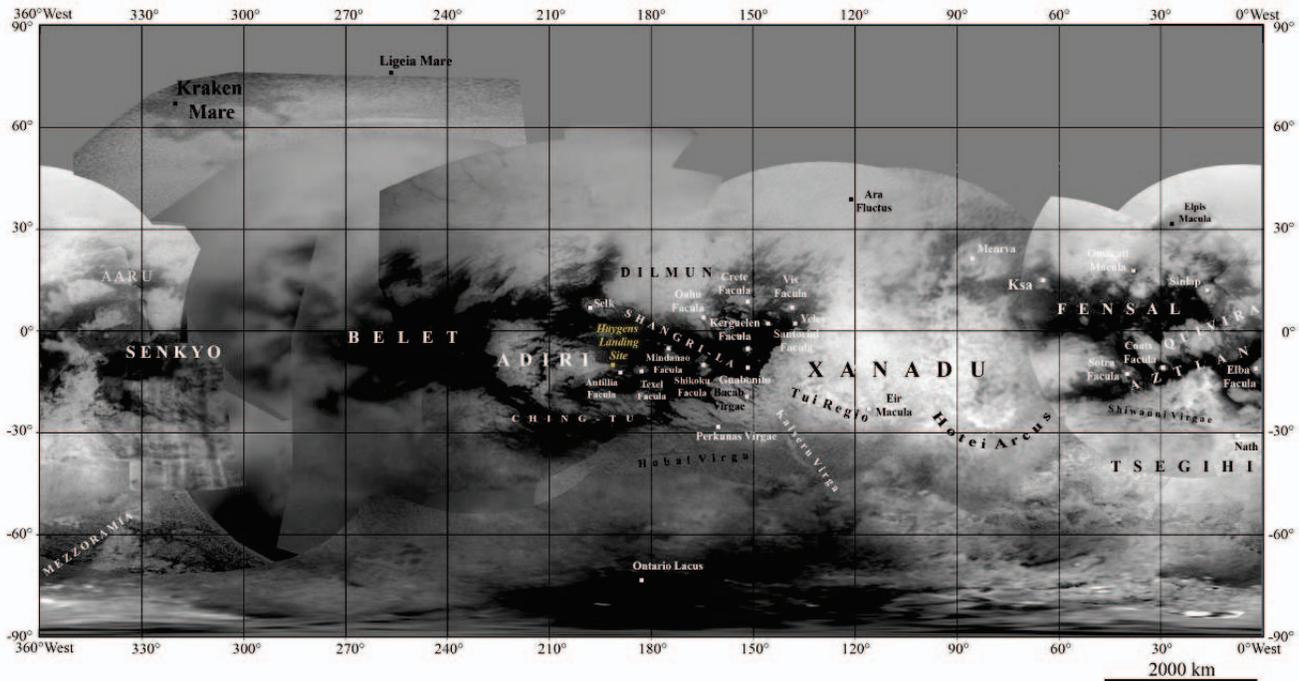
Figure 1. Cassini Imaging Science Subsystem (ISS) camera map of Titan from 2011 (Credit: NASA/JPL/Space Science Institute). Due to flyby geometries, global coverage - especially in northern polar regions - is patchy and at varying resolutions, limiting the usefulness for science.

2 AU, so a chemical system must be used after that).

3. Trajectory options also define the Earth departure energies (C3), which are then used in the selection of appropriate launch vehicles for a given injection mass. The overall space system mass is first estimated using parametric formulas, until a suitable mission is identified, at which point the system can be sized in more detail (an iterative process in itself).

This entire process is usually iterated multiple times to converge on an acceptable solution, in terms of launch mass and flight time. Adding additional options such SEP (solar electric propulsions, described below) may expand the solution space. Once the arrival date is set, a second and third set of calculations must begin to determine the orbit insertion (aerodynamic flight) and then the station keeping during the duration of the mission.

Propulsion

ΔV requirements and delivered mass are essential inputs into the choice of a propulsion system. Furthermore, there are several options that can be considered depending on the mission stage. For the interplanetary (cruise) stage, propulsion may be one or more of three types: (i) combustion engine with traditional fueling (hypergolics, e.g. MMH-NTO[2]); (ii) engines using cryogenic fuel (LH2-LOX[3]); (iii) SEP - Solar Electric Propulsion (ion propulsion, by electric ionization and acceleration of heavy elements such as Xenon). Despite the 'wet' mass savings of switching from the traditional hypergolics to the higher impulse cryogenic fuels (I_{sp}=420 s for LOX/LH2 versus 320 s for MMH/NTO), and especially

[2]Mono-Methyl Hydrazine fuel with Nitrogen Tetra-Oxide oxidizer.
[3]Liquid hydrogen stored at 16–20 K, and liquid oxygen.

to the SEP propulsion, there are disadvantages. For outer solar system missions the solar panels required for SEP grow quadratically in size with distance from the Sun, quickly erasing wet mass savings, while long-term storage of cryogenic fuels has not yet been demonstrated in space (large cryogenic rockets, such as the Delta IV, are fueled on the launch pad and the fuel is immediately used in leaving Earth). For these reasons, hypergolic engines are preferred for the cruise part of the mission. To reduce wet mass, gravity assists at Venus and Earth were used to decrease C3 from $\sim$90 to $\sim$14 km^2/s^2, noting that unfortunately Jupiter is not in the right position to provide a gravity assist for launches in the early 2020s.

For orbit insertion at Saturn and eventually Titan, the same options are available ((i)–(iii) above) plus (iv) - aerocapture, use of the planet's/moon's atmosphere to provide the required velocity change ΔV to achieve orbital insertion. In the current study, the aerocapture mission architecture was selected, to compare mass savings to previous studies that featured propulsive capture, but required larger launch C3s.

Interplanetary Flight Dynamics

The Titan transfer trajectory takes the form of a Saturn mission design with unique arrival constraints to ensure a minimally energetic arrival requirement and geometric conditions. Several transfer options are available which use multiple Earth and Venus flybys to achieve the needed C3 energy to raise aphelion to the Saturn orbital radius. Shown in Fig. 2 are three options which utilize two Earth flybys and an optional Venus gravity assist. A trade between the transfer time, V_{inf}, and Titan aerocapture entry velocity yields the baseline design with a launch date of October 25, 2021 (Fig. 3). Based on an Atlas-V class launch vehicle, a reasonable launch C3 of

Table 1. TOPS mission science traceability matrix.

Science Objectives	Measurement Objectives	Measurement Requirements	Instruments	Instrument Requirements	Mission Requirements	Data Products
A. Determine the age, and history of Titan's surface, and relative importance of exogenic versus endogenic processes in the past.	Global topographic mapping to determine surface topography/terrain	Altimetry at 1 m altitude, and 1-2 km lateral resolution	RADAR Altimeter (c.f. TIPEX RADAR)	X-band RADAR, 1.5 km lateral/1m altitude resolution 20 km swath	800 orbits at 50% duty cycle, 1500 km range. 20 kg 38W (53 W peak)	>99% global coverage RADAR altimetry maps (3 kbps)
	Morphology of craters, dunes, rivers; extent and shorelines of lakes; search for tectonic features.	200 m resolution global mapping	RADAR SAR (c.f. TIPEX RADAR)	X-band RADAR, 100 m spot size, 27 km swath	800 orbits at 50% duty cycle, 1500 km range. 20 kg 38W (220 W peak)	>99% global coverage RADAR SAR maps (85 kbps)
		Global imaging at 2.05, 2.73 and 5.35 microns, 50 m resolution	Imaging camera (HIRIS: MOC)	3x2048 pixels, 50 km swath, 25m/pixel	28 W 28 kg	>99% global 3-color imagery mapping (77 kbps)
B. Determine whether active endogenic actvity is continuing at the present day.	Measure the ice shell thickness to search for fissures and plutons (near surface liquids.)	1-2 km along-track, 10 m vertical resolution in ice shell (3-5 km depth or 100 m (30-50 km depth)	Ice-penetrating RADAR (c.f. TIPRA: MARSIS/SHARAD)	>20 Mhz RADAR, 10 Mhz bandwidth	10 m dipole antenna, 11 kg, 25 W (100 W peak)	Global altimetric (20-30 kbps) and ice-shell thickness measurements (280 kbps)
	Map Titan's gravity field to determine interior structure	Two-way X and Ka capability	Radio science doppler tracking	Ka stability of 10(-15) over 1000 s.	USO board, accelerometers, HGA	6th order measurement of Titan's gravity field
C. Determine the chemical composition of surface ices and organic materials.	Global multi-spectral mapping in near-IR to cover important bands of organic compounds.	1-6 micron mapping through methane windows	Near-IR spectral mapper (HIRIS: VIMS/MMM/CRISM)	1-6 micron coverage, 256 channels, 250 m/pixel 128 km swath. 120 K optics, 70 K MCT detectors	(Combined with imager)	Hyper-spectral image maps of Titan's surface, >99% coverage (225 kbps)
D. Elucidate the atmospheric vertical structure, including temperatures and hazes.	Measure the vertical structure of haze layers	Global imaging at 2.05, 2.73 and 5.35 microns, 50 m resolution	Imaging camera (HIRIS: MOC)	3x2048 pixels, 50 km swath, 25m/pixel	28 W 28 kg	>99% global 3-color imagery mapping (77 kbps)
	Measure the atmospheric vertical temperature/pressure profile	Atmospheric refractivity profile from 200 km to surface	Radio science system	Ka stability of 10(-15) over 1000 s.	HGA antenna, Earth pointing stability of 0.05 degrees	2 temperature/pressure profiles per orbit
E. Characterize the interaction of Titan with the solar wind and Saturn magnetosphere.	Measure the spatial and temporal distribution of the magnetic field in relation to Saturn and the Sun.	In-situ magnetic field measurements	Magnetometer	range +/- 50 mT; resolution 0.05 nT, 0.05s; Sensitivity 0.1 nT	magnetometer boom (3.5 m), plus 2 kg, 2.5 W	3-D magnetic field maps (4 kbps)

$13.49 \text{ km}^2/\text{s}^2$ was selected. A C3 dispersion of $\pm 0.15 \text{ km}^2/\text{s}^2$ ($>> \pm 50$ m/s at injection) was assumed for this study. Our baseline uses an Earth-Venus-Earth-Earth-Saturn (EVEES) design with an arrival in the Saturn system in January 2031, a ten year transfer duration. Our trade parameters included the total C3, with a range of 10–90 km^2/s^2, deterministic ΔV from 600–900 m/s, and transfer durations from 8 to 14 years, with the viable options shown in Fig. 2. A mission ΔV requirement of 676 m/s is required for this design with 413 m/s allocated to the carrier for the transfer trajectory phase and 263 m/s allocated to the orbiter for aerobraking trim, apside control and orbit maintenance. This design does not explicitly include transfer statistical maneuver ΔVs other than launch vehicle dispersion corrections, but they are estimated from operational missions to be minimal, with an additional 50 m/s budgeted for the entire transfer. The baseline trajectory timeline is provided in Table 2. The percent mass estimate for fuel is ~19%.

The transfer was also based on the geometry of the arrival asymptote vector. The arrival at Saturn periapsis was timed to encounter Titan at that geometry as shown in Fig. 4. This geometry permits a polar orbit plane orientation of the Titan insertion while accounting for the gravitational perturbations of both Titan and Saturn. Note that this design did not enter into a Saturn orbit first in an attempt to reduce ΔV using the Saturn gravity well. With this direct to Titan transfer requirement a longer duration was used to reduce the arrival V_{inf}, both at Saturn and at Titan. The perturbation and system

Table 2. TOPS mission timeline.

Event	Date	Value
Launch	Oct 25, 2021	C3=13.49 km^2/s^2
Venus flyby	Feb 1, 2022	6862 km altitude
Deep space maneuver	Sep 8, 2022	52 m/s
Earth flyby	Jun 13, 2023	915 km altitude
Deep space maneuver	Nov 15, 2024	250 m/s
Earth flyby	Jun 19, 2025	676 km altitude
Deep space maneuver	Jun 29, 2026	31 m/s
Arrive Saturn system	Jan 2, 2031	n/a
Titan final approach	Jan 6-7, 2031	n/a
Orbit separation	Jan 6-7, 2031	Titan periapse -12 hr
Orbiter divert burn	Jan 6-7, 2031	20 m/s
Orbiter aerocapture	Jan 7, 2031	350×6000 km orbit

models used in this analysis included De421 ephemeris data, spice files for Titan orbital data, high fidelity gravitational models, and solar radiation pressure (srp) accelerations and integrators (RK8/9) within the Astrogator Utility of the STK software. Maneuvers are modeled as impulsive velocity corrections in a differential correction process. An optimal design which minimized ΔV magnitudes and transfer durations for placement of the Earth and Venus flybys was completed using MaNE and SwingbyCalc. These optimal transfers were then simulated using high fidelity models to
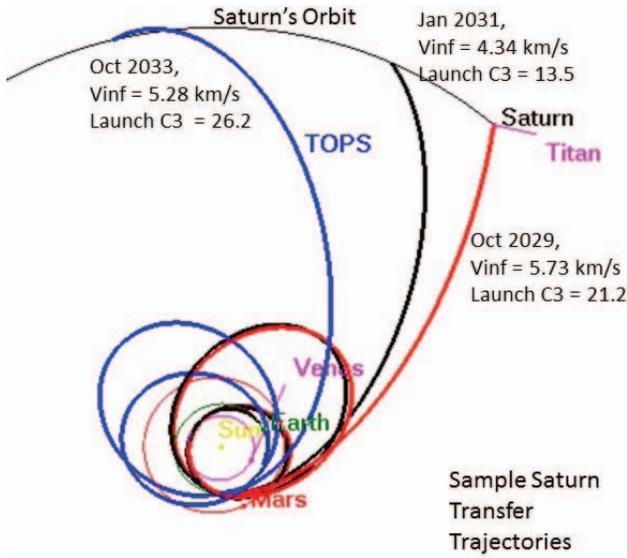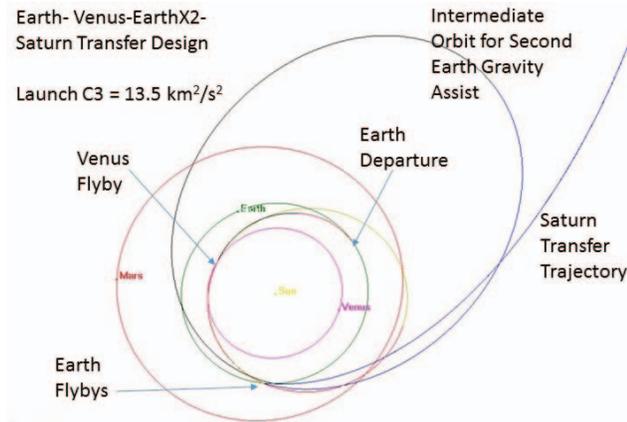
Figure 2. **TOPS transfer options.**

Figure 3. **Earth-Venus flyby view.**

generate several baselines.

Aerocapture entry and orbital maintenance

With arrival V_{inf} values and incoming asymptote vectors managed by the transfer design, the aerocapture flight path and entry corridor was studied and modeled for a range of ballistic coefficients to analyze the myriad of aerocapture apoapses, induced aerocapture ΔVs with respect to periapse altitude and accelerations (Earth g's) induced on the aeroshell capsule. The study uses an atmospheric model whose density is a function of Titan's atmospheric altitude [20]:

$$\vec{a}_{\text{drag}} = -\frac{1}{2}\frac{C_{\text{D}}A}{m}\rho v_{\text{rel}}^2 \frac{\vec{v}_{\text{rel}}}{|\vec{v}_{\text{rel}}|} \tag{1}$$

where:

$$\rho = \begin{cases} \rho_0 e^{-\beta_0(r-R)} & \text{if } r < 120 \text{ km} \\ \rho_1 e^{-\beta_1(r-R)} & \text{if } R+120 < r < R+1200 \text{ km} \\ 0 & \text{if } r > 1200 \text{ km} \end{cases} \tag{2}$$
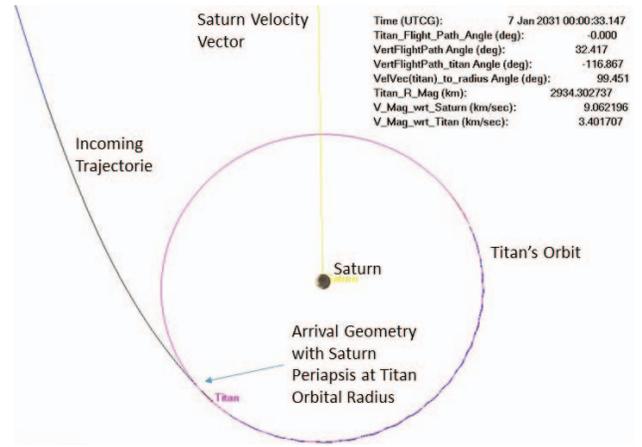

Figure 4. **Titan arrival view.**

where the density ρ varies (i.e with ρ_n and β_n values) with respect to altitude. A Monte Carlo analysis for the aerocapture entry was performed by drawing samples from a preliminary case to study the limitations and accessibility of the entry (see Fig. 5). Multiple incoming transfer design values (V_{inf}, altitude, flight path angle, etc.) were used as initial conditions with variations applied via a 3-σ estimation process. This was done in MATLAB using loaded spice kernels for the leap seconds kernel, the planetary ephemeris de421.bsp SPK files for the third body perturbations from the Sun and Saturn. The integrator used is the variable-step Runge-Kutta numerical differential equation solver ode45 function in MATLAB.
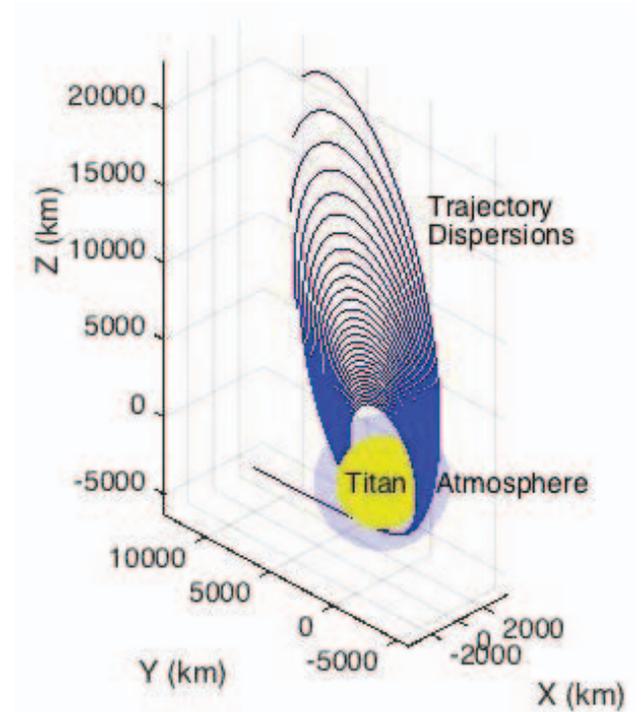

Figure 5. **Trajectory dispersions for aerocapture corridor analysis.**

The trajectory dispersion analysis provided entry constraints for the aerocapture corridor, the induced average ΔV from aerocapture as well as the time constraints after aerocapture before succumbing to Titan's atmospheric drag and gravity
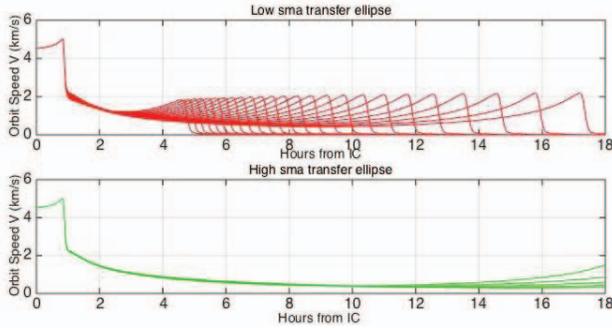
(see Fig. 6).

Figure 6. **Aerocapture ΔV and safe-hours after capture before zero speed is reached.**

A key parameter in our study was the range of feasible ballistic properties versus the incoming altitude that permitted both the capture and the subsequent aerobraking. Fig. 7 shows the ballistic coefficient ranging from 60 kg/m^2 to 114 kg/m^2, corresponding to an altitude range from 325 km to 365 km. The Monte Carlo analysis, along with the high fidelity simulations, were used to determine the thermal and system properties and constraints.
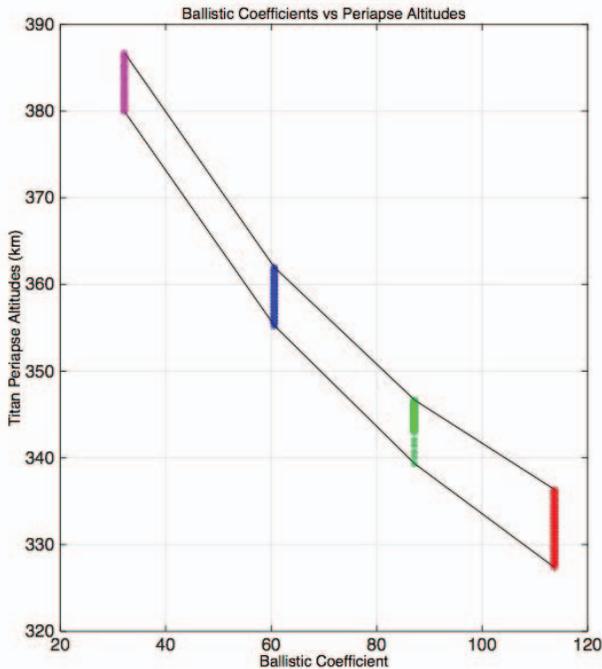

Figure 7. **Ballistic properties and captured altitude.**

Once the timing for arrival at Titan was achieved, we then focused on; minimizing arrival velocity, achieving a stable aerobraking radius, and meeting insertion conditions that included entry angles, velocities, atmospheric density, and heating. Figure 8 shows the arrival, aerocapture orbit, aerobraking orbit decrease in the apoapsis, and the final maneuver to place the spacecraft into the circular 1500 km polar science orbit. The Monte Carlo analysis provided an optimal design and the desired target conditions which were then inputed as the final arrival conditions in later high fidelity simulations.

The ΔV requirements to control the aerobraking phase are
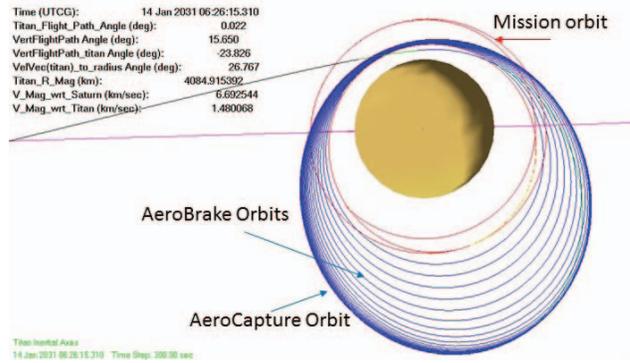

Figure 8. **High fidelity orbit capture, aerobraking, and final circularization.**

163 m/s with 20 m/s allocated to aerobraking trim and 143 m/s for the apoapsis trim and the periapsis raise. A study to determine the possible aerobraking design with various flight path angles gave us a wide range of insertion options. To model the aerobrake process, an exponential atmospheric model (Eqn. 2) was used with the transfer arrival velocity (V_{inf}), and angle of the incoming asymptote with respect to a Titan radius at periapsis. The entry code was developed separately and then the values used as initial conditions in the high fidelity simulation. Several orbit insertion conditions were traded, which determined the final orientation of the orbit to meet the insertion condition of the aeroshell and to meet the ΔV needs. This orbit requires maintenance as the Saturn and Titian gravitational perturbations result in inclination and eccentricity changes. Figure 9 represents orbit maintenance for 22 months with total ΔV of approximately 100 m/s. The maintenance was achieved by a simple re-circularizing of the orbit to a low eccentricity.
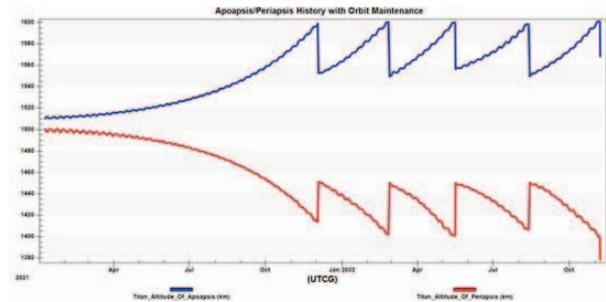

Figure 9. **TOPS orbit maintenance.**

TOPS Optical Navigation

For accuracy before separation, we need to ensure that our target will fit in the aerocapture corridor within the 8 km bound for the nominal trajectory and an apoapsis altitude of 6000 km. In order to meet these constraints, Optical Navigation (OpNav) images taken from visible-light camera(s) onboard the carrier spacecraft [4] will be used to supplement traditional radiometric tracking in the navigation solution [21]. OpNav is a common data type for interplanetary and small body rendezvous [22] [23] [24], and was recently used for the New Horizons encounter at Pluto [25]. OpNav image processing begins shortly after acquisition of the Saturn system. Acquisition is defined as the point where the apparent magnitude of Saturn is such that it is possible to distinguish the unresolved

[4]These could be duplicates of the orbiter camera, or less capable COTS (commercially available) cameras.

planet in the image from the noise of the imaging sensor. The center of the planet in the image (centroid) provides a direct measurement of the angular position of the spacecraft with respect to Saturn. Centroid measurements are typically accurate to less than one pixel. Once Saturn becomes fully resolved in the image, the apparent diameter of the planet provides spacecraft-to-Saturn range information in addition to the relative angular measurement [26]. The centroid and apparent diameter OpNav measurements ensure the correct spacecraft approach vector upon entering the Saturn system.

Titan-relative OpNav begins as soon as the moon is acquired and distinguishable from Saturn. Similar to the Saturn-relative OpNav procedure, centroid and apparent diameter measurements provide spacecraft-Titan relative position information that enables precise targeting of the aerocapture corridor. Our OpNav concept is shown in Fig. 10. Additional analysis is required to ensure that the entry corridor constraints can be met.
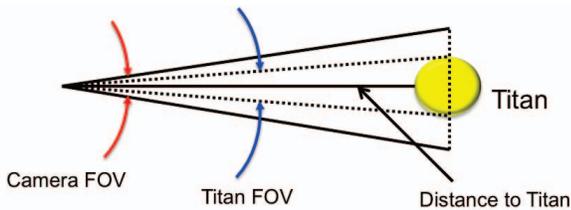

Figure 10. TOPS optical navigation concept.

4. MISSION SYSTEMS ENGINEERING

The entire mission spacecraft system consists of three major elements, each with a specific purpose: (i) the Titan orbiter with scientific payload, that is dormant until immediately after the aerocapture maneuver; (ii) the aeroshell required to protect the orbiter from heat and mechanical stresses during the aerocapture maneuver; (iii) a carrier spacecraft, to maintain the orbiter/aeroshell combination during the long cruise to Titan, and guide it into the correct entry corridor at Titan. Figure 11 shows the entire spacecraft stack that persists until final approach to Titan.
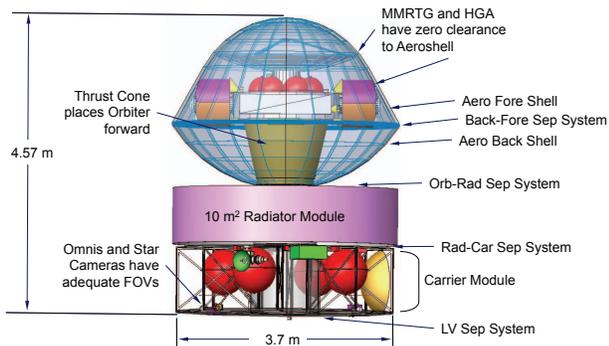

Figure 11. TOPS spacecraft stack.

The functions of each mission element are now described, followed by comments on some of the subsystems which present particular challenges for this mission.

Carrier Spacecraft

The carrier spacecraft (Fig. 12) will provide a mechanical interface to the launch vehicle for the entry shell, and will provide a method of radiating 4 kW of thermal waste heat generated inside the entry shell (radiator remains with aeroshell until atmospheric entry). It also provides adequate ADC functions to enable DDOR (Delta Difference One-Way Ranging) and eventually, optical navigation to the Titan aerocapture corridor, communications to Earth to enable adequate health and safety monitoring, and DDOR functions. The carrier spacecraft will utilize MMRTG power during the cruise phase. After separation from the orbiter/aeroshell, it will utilize a primary battery to enable critical event coverage during aerocapture. During the 2+ hour round trip light delay, the carrier spacecraft will have to provide enough autonomy, through avionics and software to accommodate guidance, navigation, health and safety, and required ΔV capability for mission operations from launch through to releasing the orbiter/aeroshell for aerocapture (including targeting maneuvers for all flybys and aerocapture). After relay of the aerocapture telemetry from the orbiter/aeroshell, the primary battery will expire and the carrier spacecraft will glide onwards but defunct outside the Saturn system.
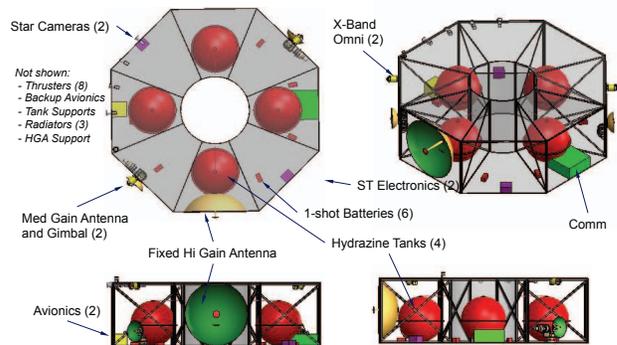

Figure 12. TOPS cruise stage.

Aeroshell

The aeroshell system will have to: protect the TOPS Orbiter during atmospheric entry, provide an appropriate L/D (lift/drag) to enable successful capture at Titan, allow the orbiter to control the attitude of the aeroshell and orbiter stack during the atmospheric encounter, allow critical events coverage to the carrier during entry phase, and provide thermal accommodation of 4 kW of waste heat for 80 minutes. The aeroshell will deploy the TOPS orbiter safely once the atmospheric encounter is complete. The aeroshell design - a crucial component of the mission - is described in more detail in Section 5.

Orbiter

The TOPS orbiter (Fig. 13) will provide the RF link to the carrier during aerocapture (required critical events coverage), execute the autonomous sequence for separation from the aeroshell, and later during the periapsis burn will provide data downlink to the Earth for DDOR and eventually, science data transmission. It will also provide power, pointing, mechanical support and thermal management for the instrument payload, as well as the avionics and software required for semi-autonomous operations.

Subsystems Challenges

Power is baselined on the use of MMRTGs, since the NASA ASRG development program has been halted. MMRTGs provide a somewhat poorer power-to-mass ratio (125 W at start of life, 45 kg, 2.8 W/kg for MMRTG; 130 W at start
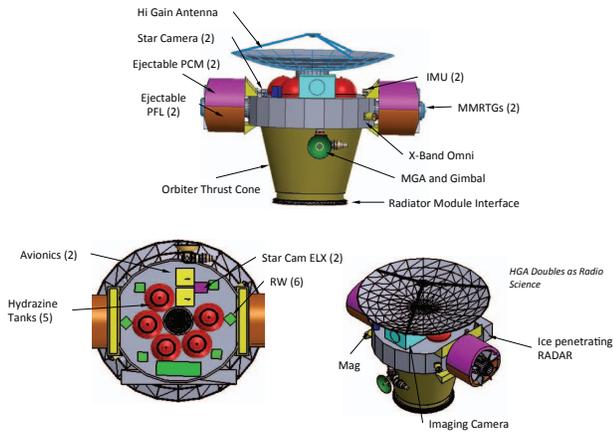
Figure 13. TOPS Titan orbiter.

of life, 32 kg, 4 W/kg for ASRGs as planned), due to lower efficiency, however have the advantage of previous flight heritage (e.g. Curiosity Rover). The baseline two MMRTGs are included in the orbiter, and provide power to the carrier spacecraft during cruise through power linkages. The 4 kW heat load produced by the two MMRTGs must be routed through the aeroshell during cruise, which is achieved through thermal straps that pass through the back clamshell and attach to a radiator unit, in between the carrier and aeroshell.[5]

After separation, the carrier is running on stored battery power, charged from the MMRTGs, while the orbiter has plenty of power but retains the problem of shedding waste heat. For this reason, the radiator module - not needed by the carrier spacecraft - remains attached to the aeroshell until the last possible moment before atmospheric entry. The orbiter must from then on endure the 80-minutes of atmospheric passage without a way to dump the waste heat - phase change material (PCM) is therefore necessary to absorb the heat.

Another key challenge for all outer solar system missions is downlink capability. The downlink rate depends on the antenna size and power, RF (Radio Frequency) band, receiver size and power, and of course the inverse square of the distance. TOPS uses a 2.25 m TWTA (Traveling Wave Tube Amplifier) HGA (High Gain Antenna) on the orbiter, with 25 W of power output at Ka band and 100 W at X-band. This provides a Ka downlink capability of 2–14 kbps to a DSN 34 m BWG (Beam Wave Guide), or an average of 232 Mb/day for a 7-hour downlink pass. Command/uplink capability is 2 kbps at X-band. The carrier spacecraft, with less intensive downlink data volume requirements, carries a similar but smaller 1.2 m HGA. In addition, both spacecraft carry 0.25 m gimbaled MGAs (medium gain antennas), capable of 650 bps uplink at X-band, and dual omni-directional antennas for full-hemisphere radio contact (e.g. for accident/anomaly recovery) capable of 20 bps to 6 AU (50% chance).

5. AEROSHELL DESIGN

The aero-shell is a cone-sphere design, a geometry typical of planetary entry vehicles and one for which empirical and theoretical data abounds. The exact geometric parameters and resulting mass were obtained after an iterative process,

---

[5]This method was also used by the Curiosity Rover during descent.

Table 3. Skip-entry analytical model results

Parameter	Value
Entry velocity	4.9 km/s
Exit velocity	1.9 km/s
Aerocapture ΔV	3.0 km/s
Titan scale Height $1/\beta$	50 km
Drag coefficient	0.7
Lift/drag	≤ 0.2
TOPS ballistic coefficient	68 kg/m^2
Pull-up (min.) altitude	342 km
Peak atmospheric density	6.2×10^{-5} kg/m^3
Critical velocity (peak heating)	3.1 km/s
Total *convective* heat load	1.4×10^8 J
Max. *convective* body ave. heat rate	88 W/cm^2
Max. *convective* stagnation heat rate	64 W/cm^2
Max. *radiative* stagnation heat rate	69 W/cm^2
Total stagnation point heating rate	133 W/cm^2

where the complete TOPS system was first estimated and refined throughout the study. A parametric mass model of the complete system was first estimated, to include the orbiter and carrier spacecraft. Successive iterations included solid model renderings of the system which were used to initially size the outer aero-shell envelope. The resulting vehicle was processed through an analytical skip-entry analysis [27], using an exponential atmospheric model and aero-thermal model approximations [20]. This process was repeated until acceptable total aero-thermal heat loads were obtained, whilst achieving the desired aerocapture ΔV. The final flight profile and convective and radiative heat rates at the stagnation point are shown in Fig. 14.

These results were used to estimate the final Thermal Protection System (TPS) material thickness and mass. The total integrated heat flux at the stagnation point is about 2,810 J/cm^2 for convection and about 2,126 J/cm^2 for radiation, or a total of 4,936 J/cm^2. Assuming the use of SLA 561 (with density of 256 kg/m^3) throughout the aero-shell, the resulting heat shield mass is about 235 kg. Table 3 summarizes key parameters from the skip-entry analytical model.

The aeroshell design is shown in Fig. 15. The forward shell thickness is about 5.4 cm, whereas the aft shell thickness is about 2.2 cm. Both are constructed from the same SLA 561 material to simplify manufacturing.

Computational fluid dynamics (CFD) analysis was carried out at several altitudes during the trajectory, and at varying angles of attack (AOA). Boundary conditions at the pull-up altitude used in the CFD calculations are shown in Table 4.

Corresponding results are shown in Fig. 16. The stagnation point pressure is relatively low at about 500 N/m^2, the back pressure mostly uniform at about 3 N/m^2, and the edge pressure about 150 N/m^2. As expected, the velocity flow field shows dramatic compression at the shock-wave interface ($\sim$0.5 m), from free-stream velocity at about 3000 m/s to near stagnation at the vehicle nose.
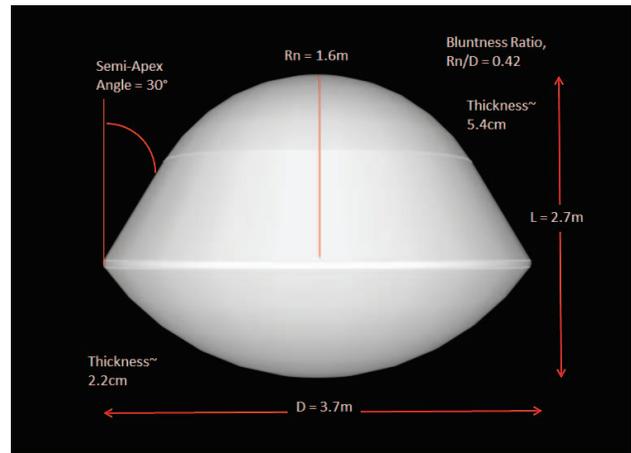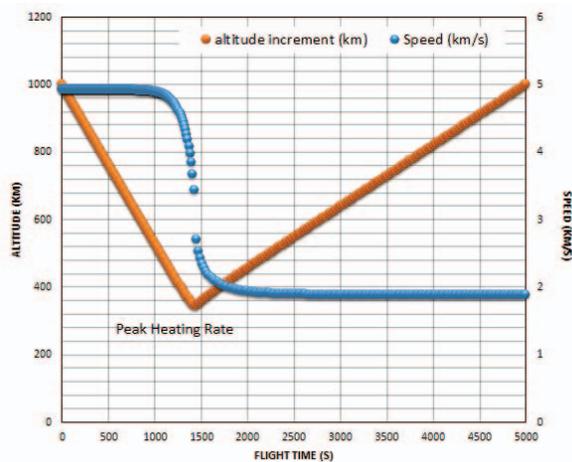
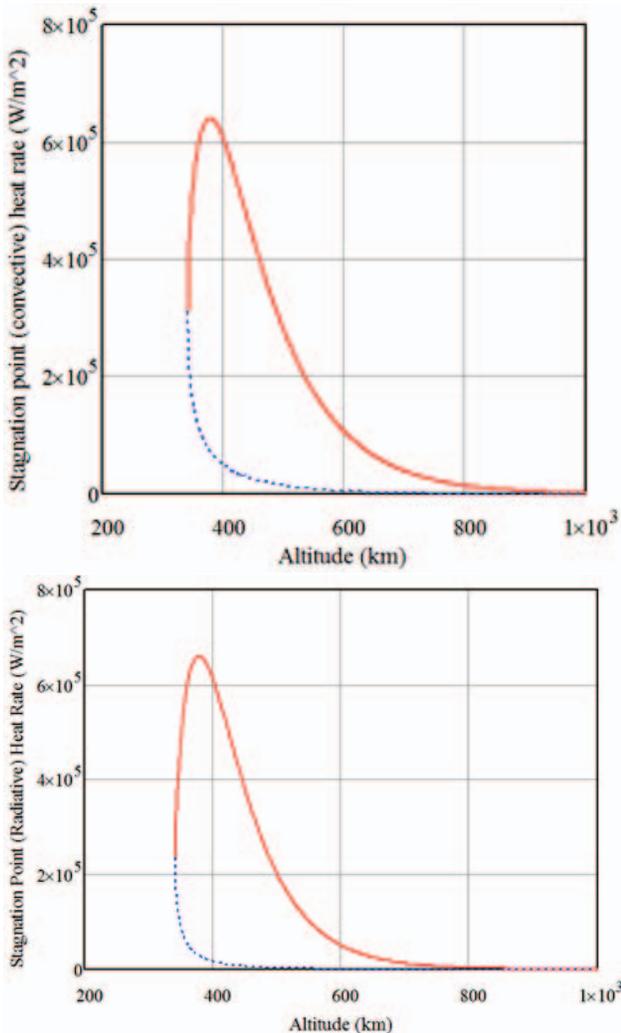Aerodynamic coefficients and moments about the about the

Figure 14. **Titan atmospheric flight analysis used in TPS system sizing. (top) Analytical skip-entry analysis; (middle) convective heat rate at the stagnation point; (bottom) radiative heat rate at the stagnation point.**

Figure 15. **TOPS aero-shell geometry.**

Table 4. **Field and system conditions at 342 km altitude (Navier-Stokes equations, compressible, viscous flow).**

Parameter	Value
Flow Velocity	3053 m/s
Density	0.0000621 kg/m^3
(Dynamic) Viscosity Co-eff.	0.00005256 kg/(m s)
Atmospheric Pressure	3.23 N/m^2
Atmospheric gas constant	299.3 J/(kg K)
Ratio of specific heats (C_p/C_v)	1.437
Angle of attack	$+5°$
Spin rate	0.175 Hz
Weight	567 N
Center of Gravity (x,y,z)	(-1.2,0,0) m
Ref. Length	2.7 m
Ref. Area	10.9 m^2

Center of Mass (CM) from the CFD analysis are shown in Table 5. Note that the lift (L) and drag (D) coefficients obtained here are a refinement over the rough approximations used in the skip entry analysis (Table 3). In reality, L/D will change during the trajectory as a result of ablation and atmospheric effects (e.g., winds and local density changes). The 10.5 rpm (0.175 Hz) spin is intended to average out some of these variations. A more detailed knowledge of atmospheric conditions will improve the initial aero-capture orbit, and more analysis is required to bound the resulting ΔV. Nonetheless, the long atmospheric flight itself will have an averaging effect on local conditions, so results here are a reasonable first approximation. Acceptable results are demonstrated for a CM axial location about 1.2 meters from the vehicle nose. Static stability conditions require that there be a restoring moment about the CM, as the vehicle strays away from a stable zero AOA attitude. A pitching moment coefficient of -0.02 corresponding to a restoring torque of -163 Nm provides a necessary indication (albeit not sufficient) the vehicle will fly stable, given the calculated mass properties.

Risks and uncertainties of aerocapture

The principal uncertainty of the aerocapture segment - besides the usual systems engineering challenges of any or-
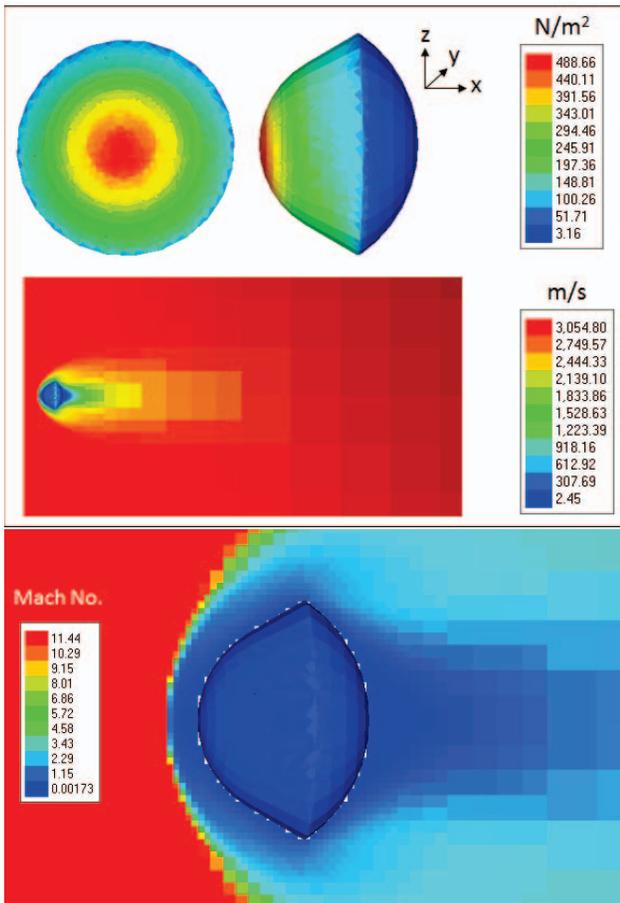
Figure 16. **CFD results at maximum density and AOA=5°.**

Table 5. **TOPS aerodynamic coefficients and moments.**

Force Coefficients	Value
Lift coefficient	0.00145
Coefficient of drag	0.832
Lift/drag	0.00174
Side force coefficient	0.00041

Moments about the Center of Mass	Value
M_x	+0.468 Nm
M_y (restoring torque)	-162.8 Nm
M_z	+0.866 Nm
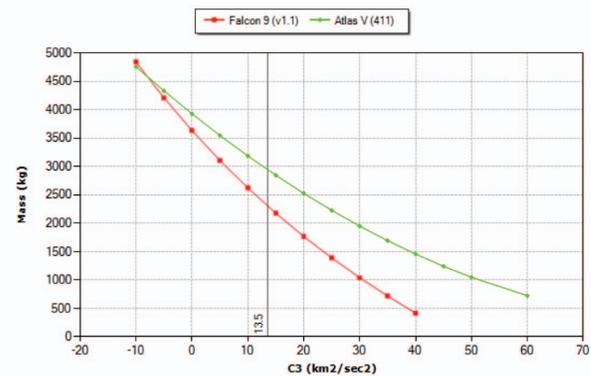
Figure 17. **Comparison of launch performance of Atlas V 411 and Falcon 9 v1.1 for TOPS.**

bit insertion maneuver such as commanding, communications, redundancy of critical systems, pyrotechnics etc - is the uncertainty in the atmospheric structure (pressure and temperature as a function of altitude at the capture point). Historically, this has been leveled as a principal criticism of aerocapture in general.

In fact, the risks are in general over-exaggerated. One useful comparison is to *aerobraking*, the slowing of an already-orbiting spacecraft to change the orbital parameters, usually to assist in circularization from a highly eccentric capture orbit. This is now a standard planned procedure used in successful Mars missions (Mars Global surveyor, Mars Odyssey, Mars Reconnaissance Orbiter) and in the later stages of several Venus missions (Magellan, Venus Express). Aerobraking occurs in the high upper atmosphere (where the spacecraft is unprotected by a heat shield), and the uncertainties are in fact much greater than for aerobraking where the retardation is primarily in the lower, denser atmosphere. This is because the upper atmosphere of a planet is less dense and more affected by solar wind pressure, expansion and contraction on daily and seasonal timescales, and other affects, and tends to be much less predictable than the middle and lower atmospheric regions which are buffered by much greater thermal inertia.

In a report on the Probablistic Risk Assessment (PRA) of propulsive capture, versus aerocapture and aerobraking at Mars [28], aerocapture was rated as slightly more reliable than aerobraking, and slightly less than propulsive capture,

which occurs in the true vacuum of space. In addition, aerocapture is likely to be much less risky than landing [29], which involves considerably greater hazards such as parachute deployments and/or heat shield jettisons in the presence of dynamic pressure, the dangers of low-speed instabilities, near-surface weather-related phenomena, and other problems.

Nevertheless, for a flight mission, accurate knowledge of atmospheric conditions in the final approach to the time of atmospheric entry would be important. This could be achieved by a combination of means: ground-based observation, measurements from another spacecraft in the Saturn system at the time of entry (if any) and/or measurements made by instruments that could be added to the cruise stage of TOPS. It should be noted however that substantial margins will necessarily be designed into an aerocapture system (as all critical orbit insertion systems) so that the aeroshell system has much greater control authority (L/D) than is anticipated to be needed; moreover, a 'failure' of the system to properly insert into a correct orbit is most likely to result in a 'poor' orbit requiring additional fuel to correct, than complete loss of the entry vehicle.

6. LAUNCH SYSTEM

The fully loaded TOPS spacecraft stack has a mass of 2270 kg, and requires a launch C3 (characteristic energy) of 13.5 km^2/s^2. The performance of two launchers considered, the Atlas V 41 and the Falcon 9 v1.1, is shown in Fig. 17.
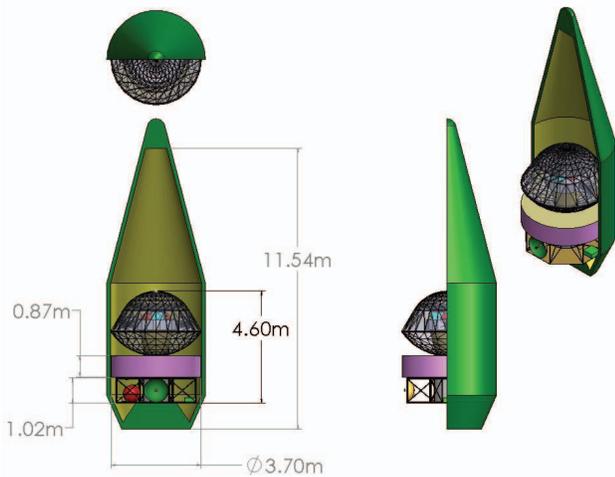
Figure 18. **TOPS Titan orbiter inside the Atlas LPF.**

For a C3 of 13.5 km^2/s^2, the Atlas V 411 can loft 2950 kg to 185 km LEO (30% margin), whereas the Falcon 9 v1.1 can lift only 2310 kg, giving a narrow 2% margin. For this reason the Atlas V 411 is the required vehicle: a larger Atlas (421, 431 etc) could give additional margin at additional cost. Fig. 18 shows the TOPS stack inside the 4m LPF (Long Payload Fairing), atop the 47" launch adaptor ring.

The fit is tight: if the aeroshell diameter grows substantially then it would be necessary to step up to the larger and more costly Atlas V 5xx series with 5m fairing.

7. MISSION OPERATIONS

The TOPS mission has been determined to consist of the following high-level phases (Fig. 19):

1. Launch and checkout
2. Venus flyby
3. Earth flybys
4. Cruise
5. Approach
6. Aerocapture and orbit adjustment
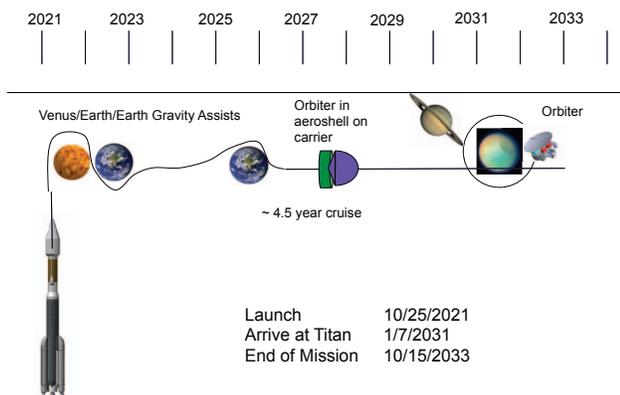7. Orbiter checkout
8. Science operations

Figure 19. **TOPS mission flight summary.**

Launch, Gravity Assists and Cruise

Post launch, the spacecraft systems undergo rigorous checkout, prior to the sequence of gravity assists. The Venus gravity assist provides the greatest thermal load of the mission, when the solar flux is double that at the Earth. Thermal systems are designed to handle this heat load. The Earth gravity assists provide a different challenge, which to manage the risk of Pu-238 entry to the Earth if the spacecraft was to suffer a failure that put it on an Earth-intercept course. This risk is managed through protection of tanks from micrometeoroids, and biasing the trajectory away from the Earth. During the remaining 4.5 years of cruise following the last gravity assist, the spacecraft will undergo period contacts with the Earth (every 2–4 weeks approx.) to monitor the health and status of spacecraft systems. During the final approach phase - prior to spacecraft separation - the optical navigation task will occur.

Aerocapture sequence

The critical aerocapture sequence proceeds as follows:

- Optical navigation: the cruise vehicle guides the spacecraft stack to the entry corridor.
- Carrier separation from the aeroshell, at approximately 12 hours prior to entry. From this point forward, the carrier spacecraft is running on battery power.
- Carrier divert maneuver, and carrier turns to track the the aeroshell position.
- Radiator assembly maintains MMRTGs at appropriate temperature prior to aerocapture phase, and remains with aeroshell until last possible moment before ejection.
- Aeroshell enters capture corridor for a duration of about 80 mins.
- Carrier monitors real time critical events telemetry, and relays to Earth on repeat cycle until batteries die.
- Aeroshell separates after atmospheric encounter.
- Orbiter calculates apoapsis safety burn.
- Orbiter establishes communication with Earth to telemeter post-aerocapture critical events.
- Orbiter performs safety burn at apoapsis.
- Orbiter aero-brakes until science orbit is reached.

A detailed timeline for the aerocapture sequence is given in Table 6 and depicted in Figs. 20 and 21.

Figure 20. **TOPS aerocapture timeline.**
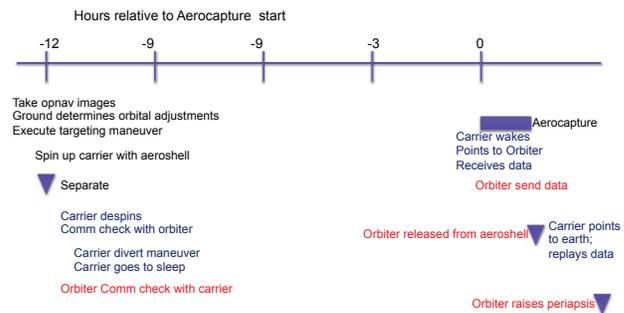
Critical Event Coverage

Critical events in the operation of a spacecraft are defined as those that must be executed successfully, usually in a single opportunity, as failure could lead to early loss or significant degradation of the mission if not executed successfully or recovered from quickly in the event of a problem.

NPR 8705.4, Risk Classification for NASA Payloads requires

Table 6. Aerocapture timeline

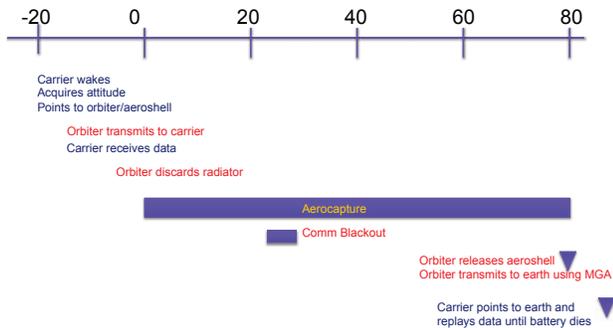| Time relative to aerocapture start	Carrier Spacecraft	Orbiter /Aeroshell
Before Separation	Collect opnav images	
	Ground computes trajectory adjustments	
	Carrier performs targeting maneuver	
12 hours	spin up carrier and aeroshell	
12 hours	Release aeroshell; de spin	
12 hours	divert maneuver	
12 hours	Comm check	Comm check
12 hours	sleep	
20 minutes	wake up; acquire attitude; point to orbiter	
15 minutes	Comm starts	Comm starts
5 minutes		Release radiators
0 minutes		Aerocapture starts
~22 minutes		Peak heating; Comm blackout; peak deceleration
80 minutes		Aerocapture ends - Release aeroshell Acquire attitude Point HGA to earth and transmit data
90 minutes	stop receiving data point antenna to earth transmit recorded data continuously until battery dies	periapsis maneuver
2.5 hours		Playback Aerocapture

Figure 21. TOPS aerocapture timeline detail.

from Earth.

Table 7. Global mapping time for each instrument.

Instrument	Swath Width (km)	Mapping Time (hrs)	Mapping Time (days)
X-band radar	20	3883	162
Camera	50	1553	65
NIR Mapper	128	607	25
IPR	10	776	324
Radio Science	N/A	N/A	N/A
Mag.	N/A	N/A	N/A

that critical event telemetry be recovered for reconstruction of an anomaly, should one occur. Critical event telemetry must be transmitted from the spacecraft in real-time, in case the RF link is lost, but is not required to be displayed or analyzed in real time. NPR 8705.4 provides examples of critical events. Critical event coverage may be provided in any fashion that is deemed appropriate for the proposed investigation.

Orbital Operations

TOPS will achieve a 4.8 hour polar science orbit around Titan at an altitude of 1500 km relative to the surface. The spacecraft will endure a 58 minute maximum occultation of Earth when the orbiter is behind Titan. Titan's orbit around Saturn is 15.94 days, and Saturn will occult Titan for about 6 hours each orbit. DSN contacts with the spacecraft will be scheduled to avoid occultations. In addition, rarer solar conjunctions will be 1 week long at point of maximum range

During the science phase, the X-band radar, ice penetrating radar and camera/spectral mapper may only be used one at a time due to power constraints. The magnetometer may be on at the same time as other instruments due to low power consumption. The instrument duty cycle is low since it will take much more time to downlink the data than to collect it. The length of the science phase is determined by the amount of time it takes to downlink sufficient data to meet the science requirements. Fig. 22 shows a concept of the weekly operations. Table 7 shows the required time for global coverage by each mapping instrument, although downlink limitations restrict the actual coverage possible.

Data downlink averages 232 Mbits per day (7 hours of downlink), meaning that on average that amount of data can be collected (after compression). Any overages cannot be
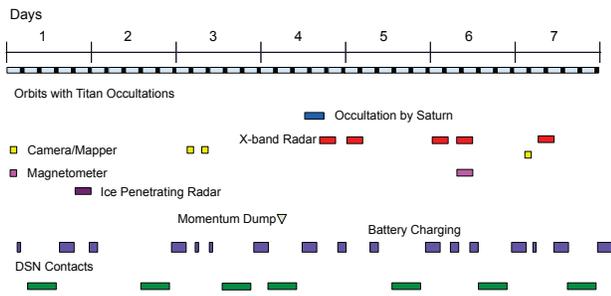
Figure 22. **TOPS weekly ops concept.**

downlinked. Working backwards from a 22-month mission duration determined earlier by station-keeping fuel costs, we conclude that a total of 155,865 Mb of data can be downlinked. In Table 8 we have sized the data collection to fit the downlink and mission duration. This shows that much less than global coverage can be expected for most instruments.

8. CONCLUSIONS

Mission Challenges

Several key challenges were apparent at the end of the mission study. Two of these are problematic to all missions to the outer solar system (power and downlink), while three are unique to the aerocapture mission architecture, and in particular the need for an aeroshell.

1. **Downlink capability:** The mission duration and % eventual surface coverage by each instrument is essentially set by the capacity of the downlink, averaging 232 Mb/day. This provides much less than global coverage for all instruments, meaning that to increase coverage either (a) the data rates or instrument complement would need to be reduced, (b) the mission duration would need to be in increased or (c) the downlink rate would need to be increased. A larger and/or more powerful antenna system, or larger ground station capability (e.g. DSN 70 m, or arrayed 34 m antennas) would provide additional downlink capacity that could translate into improved surface coverage and/or a shorter mission duration.
2. **Power:** The MMRTGs are less powerful (125 W vs 130 W) and heavier (45 kg versus 32 kg) than the planned ASRGs. Lighter and/or more powerful units would permit mass savings or more power for communications and instruments.
3. **Thermal:** The 2 kW waste heat per MMRTG unit (4 kW total) is a major problem for the aerocapture architecture, requiring the addition of a large, detachable radiator unit, and phase change material for the atmospheric passage (n-octacosane, ∼40 kg).
4. **Optical Navigation:** As described in §3, considerable attention must be given to optical navigation prior to carrier/orbiter separation, to ensure that the required 8 km entry corridor can be targeted, since the probe is unable to change course after separation, until atmospheric entry.
5. **Critical events coverage:** The requirement of continuous telemetry monitoring from the orbiter/aeroshell during the aerocapture mission phase necessitates a more complicated mission architecture, adding functionality to the orbiter and carrier spacecraft 2-way radio link, outside of heat shell, and an additional carrier divert maneuver and subsequent downlink of the telemetry data to Earth.

Mission Trade Study

At the conclusion of this study, we tried to answer the question as to whether the additional complexity of an aerocapture mission is justified in terms of substantial savings in mass, and therefore reductions flight time, launcher size, or increases in payload size, etc. Although resources did not permit a fully functionally equivalent design study for a 'traditional' (propulsive, using hypergolics) mission architecture, we attempted to compare the parameters of the aerocapture design to a previous, limited scope parametric study for a propulsive Titan orbiter, completed at GSFC in 2012. The parameters of both missions are listed in Table 9.

It is important to note that the mission designs are not fully equivalent, as there were different payload mass assumptions and launch dates - although both included a EVEES trajectory with three gravity assists. The TOPS-Trad mission also used ASRGs for power, whereas the TOPS-Aero assumed the heavier and less efficient MMRTGs. Note that the ΔV for the TOPS-Aero is the propulsive ΔV required - an additional 2.6 km/s is included in the aerocapture maneuver, which results in the substantially greater fuel load for the TOPS-Trad version. Overall, it appears likely however that the TOPS-Aero does result in a substantial mass saving, as the increase in dry mass is more than compensated by the decrease in fuel mass. For comparison, an earlier study [5] found that aerocapture offered an even more dramatic 280% mass advantage for an aerocapture Titan mission, over a similar propulsive-capture mission.

Conclusions and Further Work

This paper has described the outline parameters of a small, lightweight Titan aerocapture mission. This expands on previous studies of larger 'flagship' size Titan aerocapture orbiters. Much further work would need to be completed to bring this to the level of a fully implementable mission. However, we draw several broad conclusions. First, that aeroacapture can offer substantial mission advantages for mass reduction. Second, that even at this reduced size, and using the canonical $1M/kg (dry mass) rule-of-thumb cost estimate, we deem it unlikely that a Titan orbiter mission can be flown within the constrained budget of a Discovery mission. However, it is not unfeasible that such a mission could fit into a New Frontiers class of mission, depending on how launch costs and Phase E (operations) were accounted for. Further mission designs and refinements should also focus on increasing data downlink rate, and power/mass ratio of RTG power sources - both highly mission-enabling for outer planet missions.

ACKNOWLEDGMENTS

REFERENCES

[1] H. B. Niemann, S. K. Atreya, J. E. Demick, D. Gautier, J. A. Haberman, D. N. Harpold, W. T. Kasprzak, J. I. Lunine, T. C. Owen, and F. Raulin, "Composition of Titan's lower atmosphere and simple surface volatiles as measured by the Cassini-Huygens probe gas chromatograph mass spectrometer experiment," *Journal of Geophysical Research (Planets)*, vol. 115, pp. 12 006–

13

Table 8. TOPS Mission Data Budget

Instrument Type	Mode	Hours For 100% Coverage	Coverage Factor	Actual Hours	Data Rate (kbps)	Data Volume (Mb)
X-band radar	SAR	3883	0.01	39	85	11,882
	Altimeter	3883	0.50	1942	3	20,968
Vis/NIR	Camera	1553	0.03	47	77	12,915
	NIR Mapper	607	0.03	18	225	14,750
LW radar	Altimeter	7766	0.01	78	25	6,989
	Ice Crust	7766	0.01	78	280	78,281
Mag.	Mag.	10000	0.07	700	4	10,080
Total						**155,865**

Table 9. TOPS Mission Architecture Comparison

Mission Type	Launch Date	Flight Time	ΔV (m/s)	C3 km^2/s^2	Launch Mass (kg) Dry†	Fuel	Total (Wet)	Payload Mass (kg)
TOPS-Trad	02-Feb-2022	10.75	3427	27.2	917 (43%)	2023 (0%)	2940	15
TOPS-Aero	25-Oct-2012	9.25	666	13.5	1784 (30%)	484 (0%)	2268	75

† Mass margin/contingency included in mass estimates are shown below as a percentage.

+, Dec. 2010.

[2] R. V. Yelle, J. Cui, and I. C. F. Müller-Wodarg, "Methane escape from Titan's atmosphere," *Journal of Geophysical Research (Planets)*, vol. 113, p. E10003, Oct. 2008.

[3] D. F. Strobel, "Titan's hydrodynamically escaping atmosphere," *Icarus*, vol. 193, pp. 588–594, Feb. 2008.

[4] Lockwood, M.K. *et al.*, "Aerocapture systems analysis for a titan mission," NASA Langley, Tech. Rep. NASA/TM-2006-214273, 2006.

[5] J. L. Hall, M. A. Noca, and R. W. Bailey, "Cost-benefit analysis of the aerocapture mission set," *Journal of Spacecraft and Rockets*, vol. 42, no. 2, pp. 309–320, 2005.

[6] R. D. Lorenz and J. H. Waite, Jr., "Titan Explorer Flagship Mission Study," Johns Hopkins University Applied Physics Laboratory, Tech. Rep., 2008.

[7] S. Squyres *et al.*, "Visions and voyages," National Academy of Sciences, Tech. Rep., 2011.

[8] G. Karpati, J. Martin, M. Steiner, and K. Reinhardt, "The integrated mission design center (imdc) at nasa goddard space flight center," in *IEEE Aerospace Conference*, vol. 8, 2003, pp. 3657–3667.

[9] Y. L. Yung, M. Allen, and J. P. Pinto, "Photochemistry of the atmosphere of Titan - Comparison between model and observations," *Astrophys. J. Supp.*, vol. 55, pp. 465–506, Jul. 1984.

[10] E. H. Wilson and S. K. Atreya, "Titan's Carbon Budget and the Case of the Missing Ethane," *Journal of Physical Chemistry A*, vol. 113, pp. 11 221–11 226, Sep. 2009.

[11] R. D. Lorenz, C. P. McKay, and J. I. Lunine, "Photochemically-induced collapse of Titan's atmosphere," *Science*, vol. 275, pp. 642–644, 1997.

[12] C. Sotin, R. Jaumann, B. J. Buratti, R. H. Brown, R. N. Clark, L. A. Soderblom, K. H. Baines, G. Bellucci, J. Bibring, F. Capaccioni, P. Cerroni, M. Combes, A. Coradini, D. P. Cruikshank, P. Drossart, V. Formisano, Y. Langevin, D. L. Matson, T. B. McCord, R. M. Nelson, P. D. Nicholson, B. Sicardy, S. Le Mouelic, S. Rodriguez, K. Stephan, and C. K. Scholz, "Release of volatiles from a possible cryovolcano from near-infrared imaging of Titan," *Nature*, vol. 435, pp. 786–789, Jun. 2005.

[13] R. M. C. Lopes, K. L. Mitchell, E. R. Stofan, J. I. Lunine, R. Lorenz, F. Paganelli, R. L. Kirk, C. A. Wood, S. D. Wall, L. E. Robshaw, A. D. Fortes, C. D. Neish, J. Radebaugh, E. Reffet, S. J. Ostro, C. Elachi, M. D. Allison, Y. Anderson, R. Boehmer, G. Boubin, P. Callahan, P. Encrenaz, E. Flamini, G. Francescetti, Y. Gim, G. Hamilton, S. Hensley, M. A. Janssen, W. T. K. Johnson, K. Kelleher, D. O. Muhleman, G. Ori, R. Orosei, G. Picardi, F. Posa, L. E. Roth, R. Seu, S. Shaffer, L. A. Soderblom, B. Stiles, S. Vetrella, R. D. West, L. Wye, and H. A. Zebker, "Cryovolcanic features on Titan's surface as revealed by the Cassini Titan Radar Mapper," *Icarus*, vol. 186, pp. 395–412, Feb. 2007.

[14] R. M. Nelson, L. W. Kamp, R. M. C. Lopes, D. L. Matson, R. L. Kirk, B. W. Hapke, S. D. Wall, M. D. Boryta, F. E. Leader, W. D. Smythe, K. L. Mitchell, K. H. Baines, R. Jaumann, C. Sotin, R. N. Clark, D. P. Cruikshank, P. Drossart, J. I. Lunine, M. Combes, G. Bellucci, J. Bibring, F. Capaccioni, P. Cerroni, A. Coradini, V. Formisano, G. Filacchione, Y. Langevin, T. B. McCord, V. Mennella, P. D. Nicholson, B. Sicardy, P. G. J. Irwin, and J. C. Pearl, "Photometric changes on Saturn's Titan: Evidence for active cryovolcanism,"

Geophys. Res. Lett., vol. 36, pp. 4202–+, Feb. 2009.

[15] R. M. C. Lopes, R. L. Kirk, K. L. Mitchell, A. Legall, J. W. Barnes, A. Hayes, J. Kargel, L. Wye, J. Radebaugh, E. R. Stofan, M. A. Janssen, C. D. Neish, S. D. Wall, C. A. Wood, J. I. Lunine, and M. J. Malaska, "Cryovolcanism on Titan: New results from Cassini RADAR and VIMS," *Journal of Geophysical Research (Planets)*, vol. 118, pp. 416–435, Mar. 2013.

[16] R. D. Lorenz, K. L. Mitchell, R. L. Kirk, A. G. Hayes, O. Aharonson, H. A. Zebker, P. Paillou, J. Radebaugh, J. I. Lunine, M. A. Janssen, S. D. Wall, R. M. Lopes, B. Stiles, S. Ostro, G. Mitri, and E. R. Stofan, "Titan's inventory of organic surface materials," *Geophys. Res. Lett.*, vol. 35, pp. 2206–+, Jan. 2008.

[17] E. R. Stofan, C. Elachi, J. I. Lunine, R. D. Lorenz, B. Stiles, K. L. Mitchell, S. Ostro, L. Soderblom, C. Wood, H. Zebker, S. Wall, M. Janssen, R. Kirk, R. Lopes, F. Paganelli, J. Radebaugh, L. Wye, Y. Anderson, M. Allison, R. Boehmer, P. Callahan, P. Encrenaz, E. Flamini, G. Francescetti, Y. Gim, G. Hamilton, S. Hensley, W. T. K. Johnson, K. Kelleher, D. Muhleman, P. Paillou, G. Picardi, F. Posa, L. Roth, R. Seu, S. Shaffer, S. Vetrella, and R. West, "The lakes of Titan," *Nature*, vol. 445, pp. 61–64, Jan. 2007.

[18] R. D. Lorenz, S. Wall, J. Radebaugh, G. Boubin, E. Reffet, M. Janssen, E. Stofan, R. Lopes, R. Kirk, C. Elachi, J. Lunine, K. Mitchell, F. Paganelli, L. Soderblom, C. Wood, L. Wye, H. Zebker, Y. Anderson, S. Ostro, M. Allison, R. Boehmer, P. Callahan, P. Encrenaz, G. G. Ori, G. Francescetti, Y. Gim, G. Hamilton, S. Hensley, W. Johnson, K. Kelleher, D. Muhleman, G. Picardi, F. Posa, L. Roth, R. Seu, S. Shaffer, B. Stiles, S. Vetrella, E. Flamini, and R. West, "The Sand Seas of Titan: Cassini RADAR Observations of Longitudinal Dunes," *Science*, vol. 312, pp. 724–727, May 2006.

[19] J. M. Moore and R. T. Pappalardo, "Titan: An exogenic world?" *Icarus*, vol. 212, pp. 790–806, Apr. 2011.

[20] Esper, J., "Mission Design and Technology for a Titan Aerobot Balloon System (TABS)," Ph.D. dissertation, University of Stuttgart, Institute of Space Systems, 2012.

[21] W. M. Owen Jr, "Methods of optical navigation," *Spaceflight Mechanics*, vol. 140, 2011.

[22] J. Riedel, W. Owen, J. Stuve, S. Synnott, and R. Vaughan, "Optical navigation during the Voyager Neptune encounter," vol. 90. Portland, Oregon: AIAA/AAS, 1990, p. 2877.

[23] R. Vaughan, J. Riedel, R. Davis, W. Owen Jr, and S. Synnott, "Optical Navigation for the Galileo Gaspra Encounter," ser. Astrodynamics Conference, vol. 92. Hilton Head, South Carolina: AIAA/AAS, 1992, p. 4522.

[24] S. Gillam, W. Owen, A. Vaughan, T. Wang, J. Costello, R. Jacobson, D. Bluhm, J. Pojman, and R. Ionasescu, "Optical navigation for the cassini/huygens mission (aas 07-252)," *ADVANCES IN THE ASTRONAUTICAL SCIENCES*, vol. 129, no. 1, p. 3, 2008.

[25] W. M. Owen Jr, P. J. Dumont, and C. D. Jackman, "Optical navigation preparations for the new horizons pluto flyby." Pasadena, CA: International Symposium on Space Flight Dynamics, 2012.

[26] J. A. Christian, "Optical navigation using planet's centroid and apparent diameter in image," *Journal of Guidance, Control, and Dynamics*, vol. 38, no. 2, pp. 192–204, 2014.

[27] Esper, J., "The Neptune / Triton Explorer Mission: A Concept Feasibility Study," ESA, Tech. Rep. SP-542, 2003.

[28] T. K. Percy, E. Bright, and A. O. Torres, "Assessing the relative risk of aerocapture using probabilistic risk assessment," in *41 st AIAA/ASME/SAE/ASEE Joint Propulsion Conference & Exhibit*, 2005, pp. 1–15.

[29] Munk, M. and Kremic, T. (2008, March) Aerocapture Summary and Risk Discussion. [Online]. Available: http://www.lpi.usra.edu/opag/archive_documents/ aerocaptureRisks03_08.pdf

BIOGRAPHY

Conor Nixon is a scientist in the Planetary Systems Laboratory at NASA Goddard Space Flight Center in Greenbelt, MD. He has 20 years experience in planetary science research, especially focusing on remote sensing of the atmospheres of the outer planets and Titan from spacecraft platforms such as Galileo and Cassini. He is the Deputy Principal Investigator of Cassini's Composite Infrared Spectrometer (CIRS), and has led mission design studies for future missions to Jupiter and Titan. He earned a Bachelors degree in Natural Sciences from Cambridge University in 1993, an MSc in Radio Astronomy from the University of Manchester in 1995, and a DPhil in Atmospheric Physics from Oxford University in 2001.

Jaime Esper is a Senior Aerospace Technologist / Flight Systems Designer at the NASA Goddard Space Flight Center (GSFC). He is the Chief Engineer of the NASA Space Geodesy Project, Technical Lead/Advisor of the IceCube Earth Science Mission, and Principal Investigator in GSFCs Internal Research and Development CAPE/MIRCA. Dr. Esper has 30 years of combined leadership experience in areas covering advanced space science missions and system concepts, spacecraft systems and technologies, instrumentation, spacecraft design, space mission processing and operations, launch vehicle Range operations, and planetary mission and entry probe design, analysis, and technology development. Dr. Espers interest in planetary exploration has centered in the design of mission technologies that enable cost-effective, focused investigations. He holds degrees in Physics (B.S.) and Astronomy (M.S.) from the University of Florida, Mechanical/Aerospace Engineering (M.S.) from The George Washington University, and Aerospace Engineering (Dr. Eng.) from the University of Stuttgart in Germany. He is author of over 30 publications, and 1 patent on thermal protection system material.

David Folta leads multiple NASA missions and develops innovative technologies across the mission type spectrum, provides operational navigation and guidance expertise to flight projects, and directs research topics on dynamical systems for trajectory design. He is the MAVEN Mission Design and Navigation Lead for GSFCs Mars mission, chair of the OSIRIS-Rex Flight Dynamics Engineering Panel, and is a member of international astrodynamics organizations. His innovations include Earthmoon libration orbit design and operational maintenance, autonomous formation flying of EO-1, and implementation of Sun-Earth manifold trajectory designs. Awards include NASAs premier honor, the Distinguished Service Medal, GSFCs highest engineering award, the Moe I. Schneebaum Memorial Award, and NASAs Medal for Exceptional Service. Mr. Folta is a GSFC Senior Fellow. Mr. Folta received his Bachelor degree in Physics from Kutztown University and a Masters in Mechanical Engineering from George Washington University.

Frank Kirchman is the Senior Mission Systems Engineer in GSFCs Mission Design Laboratory. He has technically led over 60 mission concept development studies. He also was the lead MSE for the GEMS and NICER Phase A studies. Mr. Kirchman was the Lead Instrument Systems Engineer for the Burst Alert Telescope aboard the Swift Observatory. He was the Thermal Systems Manager for the Rossi X-Ray Timing Explorer and the Nobel honored Differential Microwave Radiometer aboard the Cosmic Background Explorer (COBE). He received a Bachelors in Chemical Engineering from the Georgia Institute of Technology in 1982.

Alinda Mashiku is an aerospace engineer at the NASA Goddard Space Flight Center (GSFC) in Greenbelt, MD in the Navigation and Mission Design Branch (NMDB). She earned her undergraduate degree form The Ohio State University in 2007, and both MSAAE and PhD from Purdue University in 2009 and 2013 consecutively. Her PhD dissertation work was based on nonlinear estimation theory for Statistical Orbit Determination and Data Compression techniques for Non-Gaussian distributions. Dr. Mashiku was a recipient of the NASA Graduate Student Research Program (GSRP) Fellowship for 2010-2013. Her current work at GSFC include providing navigation and mission design analysis and support for the OSIRIS-REx and James Webb Space Telescope (JWST) missions, both planned to launch in 2016 and 2018 consecutively. Other research and work interests are in novel nonlinear estimation techniques for orbit determination, hybrid systems estimation theory, system fault detection and identification, aerocapture trajectory design and collision avoidance techniques in highly perturbed environments.